ACS APPLIED MATERIALS & INTERFACES

Research Article

Cite This: ACS Appl. Mater. Interfaces 2018, 10, 31892−31902

www.acsami.org

# Nanostructured Surfaces That Mimic the Vascular Endothelial Glycocalyx Reduce Blood Protein Adsorption and Prevent Fibrin Network Formation

Mohammadhasan Hedayati,[†] Melissa M. Reynolds,[†,‡,∥,⊥] Diego Krapf,[§,∥,⊥] and Matt J. Kipper*[,†,∥,⊥]

[†]Department of Chemical and Biological Engineering, [‡]Department of Chemistry, [§]Department of Electrical and Computer Engineering, [∥]School of Advanced Materials Discovery, and [⊥]School of Biomedical Engineering, Colorado State University, Fort Collins, Colorado 80523, United States

Supporting Information

**ABSTRACT:** Blood-contacting materials are critical in many applications where long-term performance is desired. However, there are currently no engineered materials used in cardiovascular implants and devices that completely prevent clotting when in long-term contact with whole blood. The most common approach to developing next-generation blood-compatible materials is to design surface chemistries and structures that reduce or eliminate protein adsorption to prevent blood clotting. This work proposes a new paradigm for controlling protein−surface interactions by strategically mimicking key features of the glycocalyx lining the interior surfaces of blood vessels: negatively charged glycosaminoglycans organized into a polymer brush with nanoscale domains. The interactions of two important proteins from blood (albumin and fibrinogen) with these new glycocalyx mimics are revealed in detail using surface plasmon resonance and single-molecule microscopy. Surface plasmon resonance shows that these blood proteins interact reversibly with the glycocalyx mimics, but have no irreversible adsorption above the limit of detection. Single-molecule microscopy is used to compare albumin and fibrinogen interactions on surfaces with and without glycocalyx-mimetic nanostructures. Microscopy videos reveal a new mechanism whereby the glycocalyx-mimetic nanostructures eliminate the formation of fibrin networks on the surfaces. This approach shows for the first time that the nanoscale structure and organization of glycosaminoglycans in the glycocalyx are essential to (i) reduce protein adsorption, (ii) reversibly bind fibrin(ogen), and (iii) inhibit fibrin network formation on surfaces. The insights gained from this work suggest new design principles for blood-compatible surfaces. New surfaces developed using these design principles could reduce risk of catastrophic failures of blood-contacting medical devices.

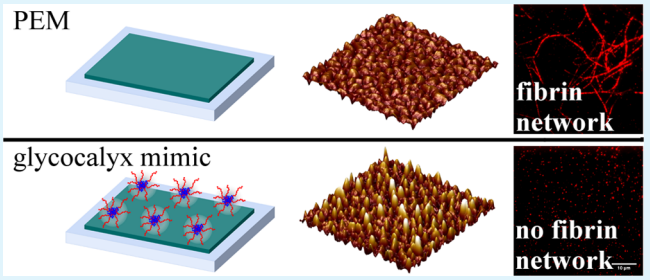


**KEYWORDS:** *single-molecule microscopy, AFM, fibrin, albumin, blood-compatible materials, polysaccharides*

## INTRODUCTION

Clotting on blood-contacting medical devices is a persistent problem, leading to catastrophic failure of cardiovascular implants and extracorporeal blood circulation devices.[1] This necessitates antiplatelet and antithrombogenic therapies for patients with devices like stents, heart valves, and shunts, and those undergoing hemodialysis and membrane oxygenation.[2] The interior surface of healthy blood vessels is the only known surface that continuously prevents blood clotting while in constant contact with flowing whole blood.[3,4]

When a biomaterial comes into contact with blood, it rapidly becomes covered with a layer of nonspecifically adsorbed proteins. This protein layer mediates the subsequent platelet adhesion, activation, and aggregation; blood coagulation is initiated and fibrinogen (FIB) is converted to fibrin monomers. These monomers subsequently polymerize into protofibrils and eventually form a crosslinked network of fibrin fibers. The resulting fibrin network supports platelet aggregates and traps red cells in a thrombus or blood clot. Protein adsorption from blood is recognized as the first key event leading to surface-induced blood clotting. Consequently, new blood-contacting materials are developed with a focus on the protein adsorption behavior at the surface.[3,5]

The surface of blood vessels prevents blood clotting by several mechanisms. Importantly, this surface stabilizes plasma proteins and acts as a barrier that blocks proteins from reaching the endothelium.[6,7] The endothelial cells lining this surface present a layer, the endothelial glycocalyx, which is rich in proteoglycans bearing glycosaminoglycan (GAG) side chains.[6,7] These cells expend energy to organize the membrane-bound proteoglycans in the glycocalyx, containing strong polyanionic GAGs, into nanoscale "bushlike" structures, 100−200 nm in diameter.[8,9] These macromolecular assemblies are organized by the underlying actin cortical cytoskeleton into

Received: June 6, 2018
Accepted: August 29, 2018
Published: August 29, 2018






DOI: 10.1021/acsami.8b09435
ACS Appl. Mater. Interfaces 2018, 10, 31892−31902

**Scheme 1. Preparation of Glycocalyx Mimics from GAG-Terminated PEMs and from PEMs Combined with GAG-Containing PCNs**

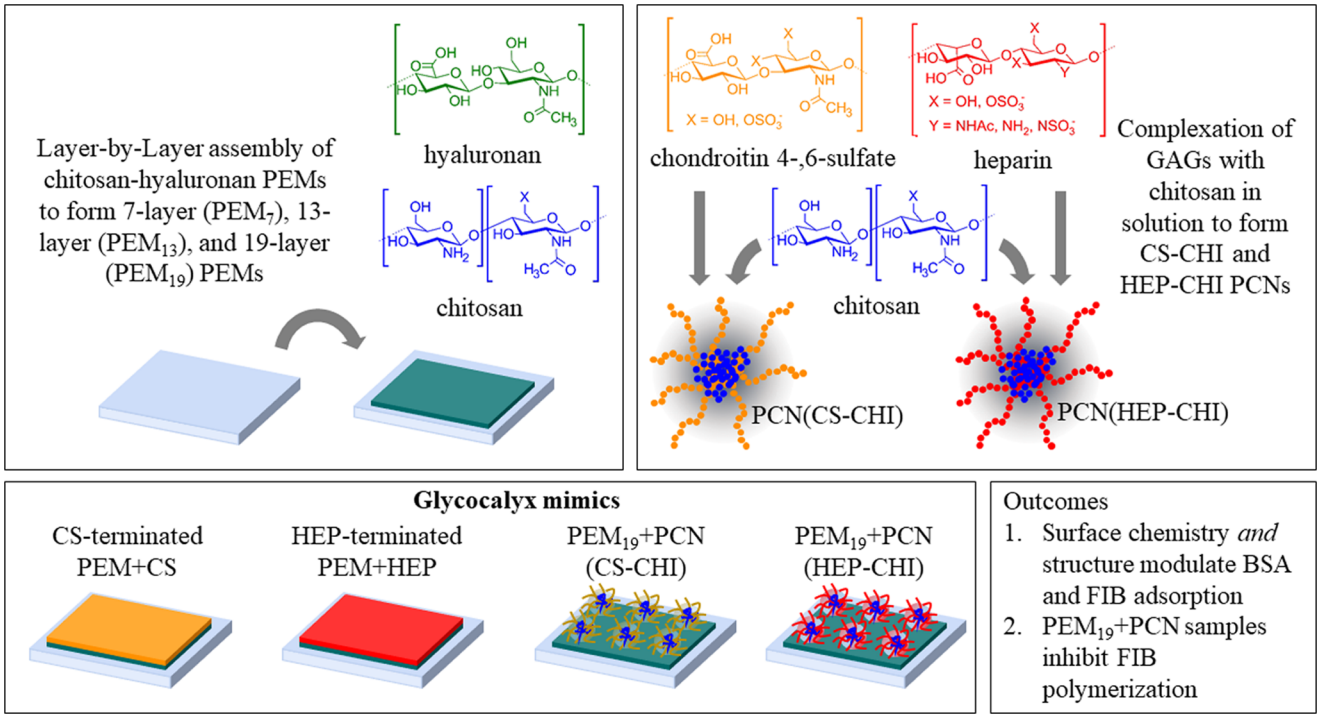


domains with 100−200 nm spacing.[8,9] We recently proposed a new method for preparing surfaces that mimic these structural features of the endothelial glycocalyx and elucidated how the preparation conditions affect the resulting structure.[10] In this work, we show that the nanoscale structure of these new surfaces suppresses nonspecific protein adsorption. Most importantly, these surfaces inhibit the formation of a fibrin network, by preventing both surface-mediated polymerization and adsorption of fibrin fibers from solution.

Heparan sulfate, chondroitin sulfate, and hyaluronan are the dominant GAGs found in the vascular endothelial glycocalyx. The current gold standard for preventing blood from clotting on surfaces of medical devices, such as blood tubing, catheters, and other blood-contacting biomaterials, is to coat the surface with the GAG heparin (HEP) (closely related to heparan sulfate).[11] Over 40 years ago, Olsson and co-workers began investigating the interactions of blood components with heparinized surfaces. They showed that heparinized surfaces could reduce platelet adhesion.[12,13] Surface-bound heparin can also inhibit thrombosis by potentiating the activity of antithrombin III and platelet factor 4.[12−17] Others have shown that heparinized surfaces may reduce fibrinogen adsorption and alter the adsorption of other blood proteins.[18] This has led to the extensive use of heparinized surfaces to improve blood compatibility of blood-contacting devices, such as dialysis membranes, venous implants, arterial shunts, microfluidic channels, vascular grafts, and arterial stents.[19−29] More recent approaches have included synthetic chemistries and superhydrophobic surfaces with nanoscale structures to prevent blood protein adsorption.[1,11,30−36]

Despite these advances, the challenges of blood clotting on biomedical material surfaces remains, in part because the mechanisms regulating blood clotting in blood-surface interactions are not completely understood.[11] We propose that by mimicking the supermolecular assembly of GAGs in the endothelial glycocalyx, we can design surfaces that reveal how blood proteins interact with the glycocalyx, and how these interactions prevent clotting. Materials that prevent blood clotting would improve outcomes and reduce risks for patients using extracorporeal blood circuits and for patients receiving cardiovascular implants.

The supermolecular assembly of highly sulfated, strong polyanions, such as heparin and chondroitin sulfate, into polymer brushes or the dense bushlike structures of the endothelial glycocalyx is energetically unfavorable due to electrostatic repulsion. We developed a technique to mimic these features on a surface and to overcome the electrostatic repulsion by polyelectrolyte complexation of polyanions with polycations, keeping the polyanions in excess.[10] We prepared polyelectrolyte multilayers (PEMs) from hyaluronan (a polyanionic GAG) and chitosan (CHI) (a structurally similar, but polycationic polysaccharide) (Scheme 1). Adjusting the pH, molarity, number of layers, and chemistry of the terminal layer can enable fine control over the PEM composition, thickness, and physical chemistry.[37,38] We also formed polyelectrolyte complex nanoparticles (PCNs) containing heparin (HEP) or chondroitin sulfate (CS) as the polyanion and chitosan (CHI) as the polycation (Scheme 1). When the polyanion was in excess, these particles formed with a collapsed core of neutralized charges, surrounded by a corona of pendent excess polyanion chains (Scheme 1). The size, $\zeta$ potential, and composition of these PCNs can be tuned by altering the charge mixing ratio of the constituent polysaccharides.[39,40] We then adsorbed CS-CHI and HEP-CHI PCNs to the PEMs to form PEM + PCN surfaces.[10,41] As we have recently reported, these PEM + PCN surfaces have 100−200 nm hemispherical bushlike domains presenting a high density of HEP or CS glycosaminoglycan chains, which mimic nanostructures in the endothelial glycocalyx.[10] In this previous


DOI: 10.1021/acsami.8b09435
ACS Appl. Mater. Interfaces 2018, 10, 31892−31902

work, we determined how the pH of the adsorption process affects the PCN coverage on 13-layer PEMs.

The outlined PEM + PCN strategy provides a new glycocalyx-mimetic surface from which the effects of nanostructure on protein adsorption can be elucidated. In this work, we study in detail the interactions of specific blood proteins with these glycocalyx mimics. We hypothesize that these new PEM + PCN surfaces can reduce the adsorption of two important blood proteins, bovine serum albumin (BSA) and fibrinogen (FIB), and that fibrin fiber network formation is modulated by the GAG-rich bushlike structures. Albumin is the most abundant protein in blood. It is amphiphilic, and its adsorption to surfaces has been promoted as a strategy for preventing platelet adhesion, since it does not contain adhesive peptide sequences. However, Latour et al. demonstrated that when albumin denatures beyond a critical degree on a surface it can promote platelet adhesion, which could lead to thrombosis.[42] Fibrinogen, a glycoprotein from blood plasma, is activated by the enzyme thrombin to form fibrin, which polymerizes to form fibers that stabilize blood clots.[43−45] Fibrin adsorption and polymerization can also be affected by surface chemistry and the orientation of the adsorbed proteins.[44,46] Therefore, controlling the specific interactions of albumin and fibrinogen with a surface may be more effective than attempting to prevent the protein adsorption altogether. To the best of our knowledge, we show for the first time that the structure of the PCNs on a surface inhibits the adsorption and formation of fibrin fibers on a surface, a key step in blood clot formation, even in the absence of the important inhibitor of fibrin polymerization, antithrombin III. This is a new mechanism of preventing blood clotting. Furthermore, these new surfaces serve as useful models for studying the structure−function relationships of the nanoscale features of the endothelial glycocalyx and provide a new strategy for designing blood-contacting materials.

## EXPERIMENTAL SECTION

**Materials.** Chitosan (CHI) was purchased from MP Biomedicals. Chondroitin sulfate sodium (CS) salt (from shark cartilage, 6% sulfur, 6-sulfate/4-sulfate = 1.24, $M_w$ = 84.3 kDa; polydispersity index (PDI) = 1.94), hyaluronic acid (HA) sodium salt ($M_w$ = 743 kDa; PDI = 1.16), bovine serum albumin (BSA), fibrinogen (FIB) from human plasma, thrombin from bovine plasma, 11-mercaptoundecanoic acid (MUA, 95%), sodium acetate, $\beta$-mercaptoethanol, catalase from bovine liver, and glucose oxidase were purchased from Sigma Aldrich. Heparin sodium (HEP) (from porcine intestinal mucosa, 12.5% sulfur) was purchased from Celsus Laboratories (Cincinnati, OH). Glacial acetic acid and ethanol (200 proof 99.5 + %) were purchased from Acros Organics (Geel, Belgium). BSA conjugated to Alexa Fluor 647 and FIB from human plasma Alexa Fluor 647 conjugate were purchased from Thermo Fisher Scientific (Waltham, MA). Phosphate-buffered saline (PBS) without $Ca^{2+}$ and $Mg^{2+}$ was purchased from Gibco (Grand Island, NY). A Millipore water purification unit was used to obtain 18.2 MΩ cm water, used for making all aqueous solutions (Millipore, Billerica, MA).

**PCN Preparation and Characterization.** PCNs formed from chitosan and GAGs were made, as previously described.[39−41,47] Briefly, chitosan, heparin sodium, and chondroitin sulfate solutions were prepared at concentrations of 1, 1.5, and 2.8 mg $mL^{-1}$, respectively, in acetate buffer solutions (0.2 M sodium acetate and acetic acid at pH 5.0). Solutions were filtered using 0.22 $\mu$m syringe filters. To prepare chondroitin sulfate-based PCNs (CS-CHI), the chondroitin sulfate solution was added to the stirring chitosan solution in a 6:1 volume ratio (36 mL of chondroitin sulfate solution to 6 mL of chitosan solution). To prepare heparin-based PCNs (HEP-CHI), the heparin solution was added to the stirring chitosan solution in a 4:1 volume ratio of heparin solution to a chitosan solution (24 mL heparin solution to 6 mL chitosan solution). The mixtures were stirred for 3 h at 1100 rpm. After 3 h of stirring, all solutions were allowed to settle overnight to remove aggregated particles. After settling, the supernatant was decanted, containing the colloidally stable nanoparticles. The aggregated particles were discarded. Dynamic light scattering (DLS) confirmed that CS-CHI nanoparticles have a reliable polydispersity index and do not require further separation. The HEP-CHI solution was centrifuged at 3000$g$ for 5 min to separate the particles from uncomplexed polymer, using an Eppendorf 5804 centrifuge. A Zetasizer Nano ZS (Malvern) was used to analyze hydrodynamic diameter using a 633 nm laser. All measurements were performed at a fixed angle of 175°, at 25 °C, in 0.2 M acetate buffer solution. Three measurements were made on each of three separate samples for each composition. The mean ± standard deviation are reported for the hydrodynamic diameter.

**Layer-by-Layer Surface Modification and Protein Adsorption by Surface Plasmon Resonance (SPR).** Polysaccharide solutions were prepared in similar acetate buffer solutions as those used for the PCN preparation (0.2 M sodium acetate and acetic acid at 5.0). This pH was selected based on our previous work.[10] Chitosan (1.33 mg $mL^{-1}$) and hyaluronan (0.66 mg $mL^{-1}$) solutions were prepared by stirring for 2 h at room temperature. Solutions were clarified by filtration through 0.22 $\mu$m syringe filters for CHI and 0.45 $\mu$m syringe filters for HA solution.

Fourier transform surface plasmon resonance (FT-SPR) was used for measuring the intensity of p-polarized light reflected from the back side of the gold film on which the samples were assembled, as a function of wavenumber, as we have described previously, using an SPR 100 module on a Thermo 8700 model Fourier transform infrared (FT-IR) spectrometer (Thermo Electron).[38,48,49] Briefly, gold-coated SF-10 glass chips (47 nm gold thickness, NanoSPR LLC, Chicago, IL) were rinsed exhaustively in ethanol, then modified with a self-assembled monolayer of MUA by soaking the gold-coated glass chip in a 1 mM MUA solution in ethanol for at least 20 h. The MUA-modified surfaces were dried with a gentle stream of dry nitrogen. MUA-modified chips were mounted to the base of a prism on one side of a flow cell, and optical contact was established between the chip and the prism using a refractive index matching fluid. A Masterflex peristaltic pump was used to pump polysaccharide and rinse solutions through the flow cell, in contact with the MUA-coated surface, with a flow rate of 0.5 mL $min^{-1}$. A low flow rate was used to ensure laminar flow over the gold chip surface. The interferometer in the FT-IR instrument was used to scan wavelengths at a fixed angle of incidence. In these experiments, FT-SPR was performed using a white light/near-infrared source with a $CaF_2$ beam splitter at the interferometer and an InGaS detector. Data were collected using Omnic 7.3 software (Thermo Electron), at 8 $cm^{-1}$ resolution from 6000 to 12 000 $cm^{-1}$. PEMs were constructed with CHI as the polycation and HA as the polyanion at pH 5.0 in the solutions described above. First, the surface was exposed to an acidified water rinse (pH 4.0, acidified with acetic acid), for 6 min. The layer-by-layer process was conducted by alternatively flowing solutions through the flow cell in the following sequence: polycation (CHI), rinse, polyanion (HA), rinse. The sequence was repeated until a 7-layer, 13-layer, or 19-layer PEM (terminating with CHI) had been adsorbed. PEM + PCN samples were prepared similarly. After the layer-by-layer assembly of 19-layer CHI-HA PEMs, either CS-CHI PCNs or HEP-CHI PCNs were adsorbed. The resulting samples are referred to as $PEM_{19}$ + PCN(CS-CHI) and $PEM_{19}$ + PCN(HEP-CHI). The length of the adsorption steps was doubled to 12 min for the PCN adsorption, followed by a final acidified water rinse. The layer-by-layer process was monitored by detecting the change in the plasmon resonance absorption wavenumber, caused by adsorption of each layer. Here, the resonance peak position in wavenumber is converted to wavelength, $\lambda_{res}$. The thicknesses of these PEM and $PEM_{19}$ + PCN samples is well within the range of sensitivity of the SPR, evidenced by changes in $\lambda_{res}$ when the rinse solution is changed.

Once the PEM and $PEM_{19}$ + PCN samples were prepared, protein adsorption was also monitored by FT-SPR. Each sample was exposed


DOI: 10.1021/acsami.8b09435
ACS Appl. Mater. Interfaces 2018, 10, 31892−31902

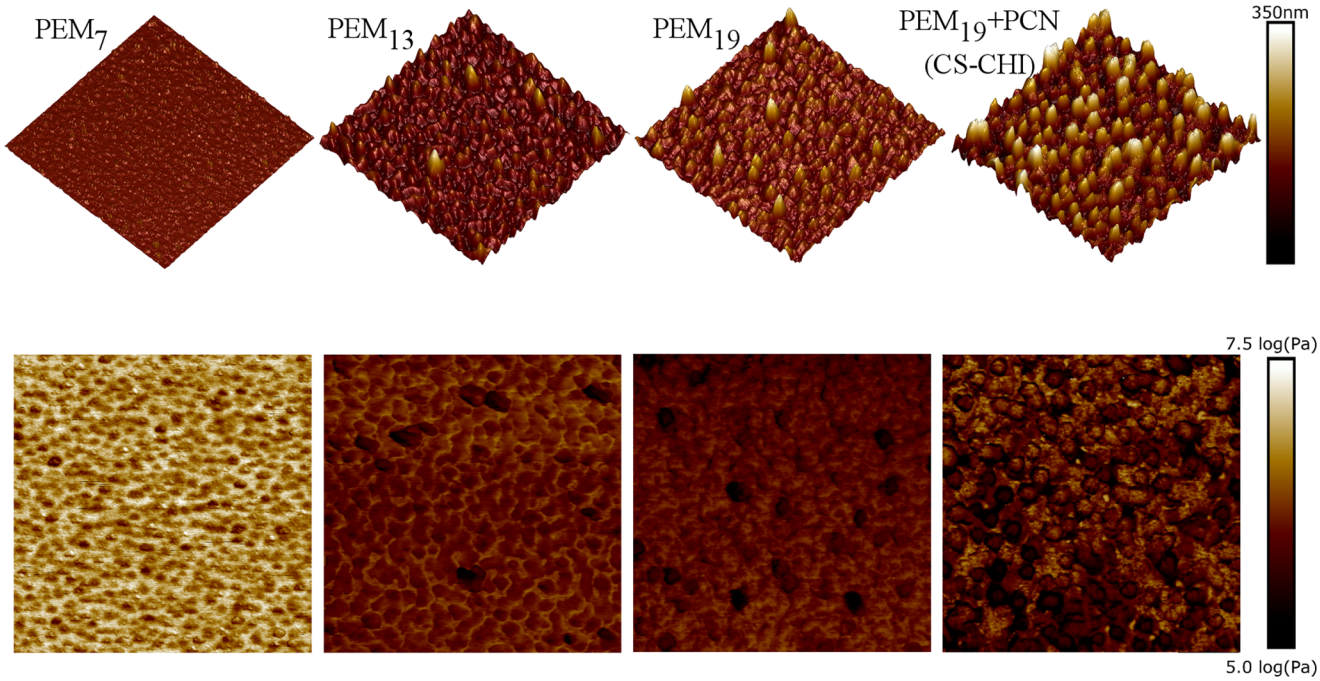


**Figure 1.** (Top) representative 5 $\mu$m × 5 $\mu$m AFM topographic images of PEMs and $PEM_{19}$ + PCN(CS-CHI) taken in liquid. (Bottom) Young's modulus (calculated using the Derjaguin−Müller−Toporov model) of representative samples shown in logarithmic scale.

to PBS for 40 min to equilibrate the surface with the ions in the buffer solution. The experiment was continued by replacing the PBS buffer with 0.75 mg $mL^{-1}$ BSA or FIB solution (approximately 12 $\mu$M for BSA and 3.5 $\mu$M for FIB) in PBS for 30 min. During protein adsorption, the plasmon resonance absorption wavelength shifts due to the difference in refractive index of the medium at the sensor surface, within the penetration depth of the SPR evanescent wave. This change in refractive index arises due to both protein deposition on the gold surface and due to the refractive index increment of the protein in solution. After reaching a steady-state value of $\lambda_{res}$, BSA or FIB solution was replaced with PBS. The amount of irreversibly adsorbed BSA and FIB was quantified as the difference in $\lambda_{res}$ measured in PBS before and after incubation with BSA or FIB solution. This difference is the $\Delta\lambda_{res}$. The average limit of quantitation (LOQ) for our instrument was estimated to be 0.1 nm, which corresponds to approximately 20 pg of deposit $mm^{-2}$.

**Atomic Force Microscopy (AFM) Measurements in Peak Force Quantitative Nanomechanical Property Mapping (PF-QNM) Mode.** The peak force QNM AFM study was done using a BioScope Resolve BIOAFM (Bruker) with Nanoscope V controller. The measurements were performed under ambient conditions at room temperature in deionized (DI) water to characterize the morphology and the mechanical properties of the sample at the nanoscale. The calibrated probe PF-QNM-LC-CAL with a tip radius of 65 nm was used, and deflection sensitivity was measured against a hard surface. The scan size was typically 5 × 5 $\mu m^2$, with a digital resolution of 512 pixel × 512 pixel, and a scanning rate of 0.5 Hz (lines per second). The oscillation frequency of the probe was set to 1 kHz, and the peak force set point was 500 pN. For every experiment, three measurements on three different samples were acquired. Image analysis was performed using NanoScope Analysis (version 1.8).

To enable imaging of PEM and $PEM_{19}$ + PCN samples by AFM in liquid, samples were prepared on glass-bottom Petri dishes (30 mm Pelco Petri dishes, Willco Wells, Amsterdam) and mounted on the AFM stage. Petri dishes were first treated with oxygen plasma for 10 min, to ensure a clean, oxidized surface. Then, layer-by-layer adsorption was conducted by exposing the glass surfaces to alternating polycation, rinse, and polyanion solutions, on an orbital shaker. The surfaces prepared on glass-bottom Petri dishes were prepared using a similar procedure as that used for the FT-SPR, listed above (polysaccharide solutions and adsorption times).

**X-ray Photoelectron Spectroscopy (XPS).** The surface chemistry of $PEM_{19}$ and $PEM_{19}$ + PCNs surfaces prepared on glass-bottom Petri dishes was evaluated by X-ray photoelectron spectroscopy (XPS). Spectra were obtained with a monochromatic Al K$\alpha$ X-ray source ($h\nu$ = 1486.6 eV), a hemispherical analyzer, and multichannel detector. High-resolution spectra were obtained using a 23.5 eV analyzer pass energy with 0.1 eV steps and an X-ray spot of 800 $\mu m^2$. All spectra were obtained with a photoelectron takeoff angle of 45°. The binding energy scales for the samples were referenced to the C 1s peak at 284.8 eV. Spectra curve fitting was done using Phi Electronics Multipak version 9.3. Elemental compositions were computed according to the atom sensitivities.

**Single-Molecule Microscopy Evaluation of Protein Adsorption and Fibrin Network Formation.** For high-sensitivity detection of protein adsorption and fibrin network formation at solid−liquid interfaces, an objective-type total internal reflection fluorescence (TIRF) microscope was used as previously described.[50,51] Specifically, the excitation was performed in oblique illumination mode for measuring protein adsorption and in TIRF mode for characterizing fibrin network formation. The samples were prepared on glass-bottom Petri dishes, as described above for the AFM characterization. The microscope was home built around an Olympus IX71 body with 638 nm laser line as excitation source (DL638-328 050, CrystaLaser, Reno, NV). A back-illuminated electron-multiplied charge-coupled device camera (Andor iXon DU-888) liquid-cooled to −70 °C, with an electronic gain of 60, was used. To maintain constant focus during the whole imaging time, we employed an autofocus system (CRISP, Applied Scientific Instrumentation, Eugene, OR) in combination with a piezoelectric stage (Z-100, Mad City Labs, Madison, WI). To reduce photobleaching, an enzymatic oxygen scavenger system was used in the imaging buffer. Imaging buffers for screening protein adsorption were 50 mM Tris−HCl (pH 8.0), 10 mM NaCl, 0.8% glucose, 0.15 mg $mL^{-1}$ glucose oxidase, 34 $\mu$g $mL^{-1}$ catalase, and 1% $\beta$-mercaptoethanol.[52] Fibrinogen from human plasma conjugated with Alexa Fluor 647 and albumin from bovine serum conjugated with Alexa Fluor 647 were used to observe protein adsorption on different surfaces. The perfusion chamber was filled with the solution containing the labeled


DOI: 10.1021/acsami.8b09435
ACS Appl. Mater. Interfaces 2018, 10, 31892−31902

protein, and after an incubation period of 10 min, with no subsequent rinse step, 105 s of microscopy videos were acquired at a frame rate of 9.5 frames $s^{-1}$, using a 100×/1.4 oil immersion objective. For each experimental condition, three independent replicates on three different samples were conducted. The protein adsorption data are reported as the mean fluorescence intensity ± standard deviation.

Fibrin polymerization was studied by mixing fibrinogen (at a final concentrations of 0.75 mg $mL^{-1}$), Alexa Fluor 647-conjugated fibrinogen (at a final concentration of 5 nM), and thrombin (at 1 NIH U $mL^{-1}$) in Tris-buffered saline (10 mM Tris, 150 mM NaCl, pH 7.4) with 5 mM $CaCl_2$, to activate thrombin at room temperature. TIRF videos were taken on at least five different regions of three different samples, and one representative image is shown here for $PEM_{19}$, PEM + CS, PEM + HEP, $PEM_{19}$ + PCN(CS-CHI), and $PEM_{19}$ + PCN(HEP-CHI). A video of these fibrin/thrombin experiments is shown in the Supporting Information.

## RESULTS

**AFM of PEM and $PEM_{19}$ + PCN Surfaces.** Atomic force micrographs (AFMs) obtained in fluid with peak force quantitative nanomechanical property mapping (PF-QNM) of the PEM and $PEM_{19}$ + PCN surfaces, prepared on glass-bottom Petri dishes (Figure 1) show that the surface roughness increases as the number of PEM layers increases. The root mean square surface roughness, $R_q$, calculated from 5 $\mu$m × 5 $\mu$m AFM images performed on triplicate ($n$ = 3) samples for each condition, is reported in Table S.1 in the Supporting Information. The apparent Young's modulus of the surface is also reduced as the layer number is increased. Furthermore, when the nanoparticles are adsorbed, they appear as approximately 200 nm diameter domains densely covering the surface. These features are similar to the sizes of the PCNs obtained by dynamic light scattering (DLS) when the PCNs are in solution (Table 1). Notably, these features have similar dimensions and spacing to the dominant GAG structures found in the endothelial glycocalyx.[8−10] Furthermore, the negative $\zeta$ potential of the PCNs (Table 1) confirms that these are enriched in the polyanionic GAGs, HEP, and CS. The AFM images also confirm the aqueous stabilities of the PEM and PEM + PCN coatings, as multiple AFM images were collected in DI water over the span of several hours, for each sample type.

**Table 1. Intensity Average Size, Polydispersity Index (PDI), and $\zeta$ Potential of PCNs**

| PCN composition | hydrodynamic diameter (nm) | PDI | $\zeta$ potential (mV) |
|---|---|---|---|
| CS-CHI | 238 ± 2 | 0.10 ± 0.02 | −30 ± 3 |
| HEP-CHI | 235 ± 5 | 0.24 ± 0.05 | −21 ± 5 |

**XPS of PEM and $PEM_{19}$ + PCN Surfaces.** To further confirm the adsorption of PCNs, X-ray photoelectron spectroscopy was performed on PEM and $PEM_{19}$ + PCN surfaces. The high-resolution scans of the N 1s and S 2p envelopes are shown in Figure 2. All samples show characteristic N 1s spectra with the amine and amide group from the polysaccharides, near 400 eV, and a strong ammonium contribution between 402 and 402.5 eV. The ammonium contribution confirms the presence of chitosan within the PEM and PCNs, as we have reported previously.[37,47,53,54] The addition of the PCN is confirmed by the strong sulfate signal in the S 2p envelope. Although the PEMs composed of CHI and HA contain no sulfate, adsorption of the CS- and HEP-containing PCNs results in a sulfur signal from the surface. The elemental compositions (C, O, N, and S) of these surfaces are reported in the Supporting Information (Table S.2). To confirm that the PEM surfaces prepared on MUA-modified, gold-coated glass are similar to those on glass-bottom Petri dishes, examples of XPS and AFM of the $PEM_{13}$ and the $PEM_{19}$ + PCN(CS-CHI) on both substrates are shown in Figures S.1 and S.2 in the Supporting Information.

**LbL Assembly of PEMs and Protein Adsorption by FT-SPR.** The layer-by-layer assembly of the PEMs, the adsorption of PCNs, and subsequent adsorption of plasma proteins were monitored by in situ Fourier transform surface plasmon resonance (FT-SPR). Layer-by-layer assembly was conducted on gold-coated glass substrates, modified with a self-assembled monolayer of MUA, as previously reported.[37,38,48] The FT-SPR data during the last steps of construction of a 19-layer chitosan-hyaluronan PEM ($PEM_{19}$), followed by CS-CHI PCN adsorption are shown in Figure 3a. During each polyelectrolyte adsorption step, the plasmon resonance absorbance wavelength, $\lambda_{res}$, increases by about 35−50 nm, due to surface adsorption and to changes in the refractive index between the rinse and polyelectrolyte solutions. Then, during the subsequent rinse step, $\lambda_{res}$, is reduced. The net change in $\lambda_{res}$ measured during the rinses before and after each adsorption step is proportional to the changes in the surface thickness and refractive index, corresponding to the amount of irreversibly adsorbed polyelectrolyte at each step.

To evaluate protein adsorption on the PEM and $PEM_{19}$ + PCN surfaces, we exposed the surfaces to solutions (0.75 mg $mL^{-1}$) of BSA or FIB in phosphate-buffered saline (PBS) for 30 min. During the protein adsorption step, the plasmon resonance absorption wavelength, $\lambda_{res}$, was monitored, as shown in Figure 3b. The wavelength is expected to shift due to the difference in refractive index of the medium at the sensor surface, within the penetration depth of the SPR evanescent field. This change in refractive index arises due to changes in the surface (e.g., protein deposition) and due to the refractive index increment of the protein in solution. In all protein adsorption experiments, the surface reaches equilibrium with the protein solution in a few minutes, suggesting that the protein−surface interaction is in dynamic equilibrium. The amount of irreversibly adsorbed BSA and FIB was quantified as the difference in $\lambda_{res}$ measured in PBS before and after incubation with BSA or FIB solution. This difference is $\Delta\lambda_{res}$. The average limit of quantitation for our instrument was estimated to be 0.1 nm, which corresponds to approximately 20 pg $mm^{-2}$ of deposit. On control surfaces (gold-coated glass modified with a self-assembled monolayer of MUA), we detected 2.2 ng $mm^{-2}$ of BSA adsorption and 3.8 ng $mm^{-2}$ of FIB adsorption. On all of the experimental PEM and $PEM_{19}$ + PCN surfaces, we detected a positive change in $\lambda_{res}$ when the surfaces were exposed to protein (between 0.5 and 2.5 nm corresponding to 0.1−0.5 ng $mm^{-2}$), which was completely reversed during the subsequent rinse. The values of $\Delta\lambda_{res}$ were either below the limit of detection or were slightly negative, indicating that the wavelength change is due to some other change on the surface. The positive change in $\lambda_{res}$ during exposure to the protein solution likely indicates reversible protein adsorption, however, no irreversible adsorption of either BSA or FIB is detected on PEM and $PEM_{19}$ + PCN surfaces. This confirms that all of the experimental surfaces are comparable to ultralow fouling surfaces.[55,56] Moreover, the inability to detect protein adsorption on PEM and $PEM_{19}$ + PCN samples cannot be attributed to the thickness of the


DOI: 10.1021/acsami.8b09435
ACS Appl. Mater. Interfaces 2018, 10, 31892−31902

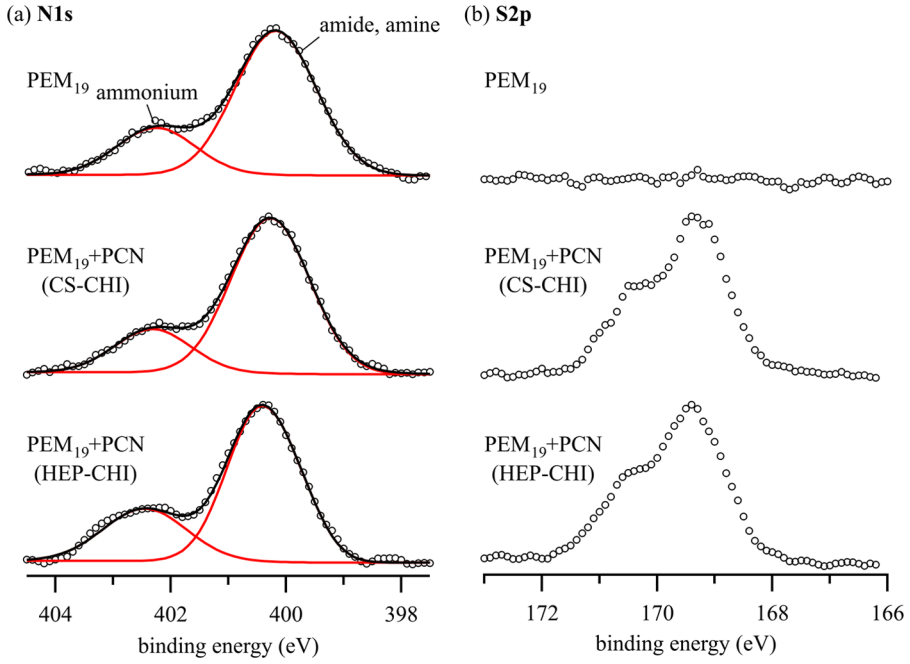


**Figure 2.** High-resolution XPS spectra of the $PEM_{19}$ and $PEM_{19}$ + PCN samples in the regions of the (a) N 1s and (b) S 2p envelopes confirm that all of the samples contain chitosan electrostatically complexed with the polyanions (evidenced by the ammonium peak) and that the $PEM_{19}$ + PCN samples contain the sulfated CS and HEP (evidenced by the characteristic sulfate signal in the S 2p envelope).

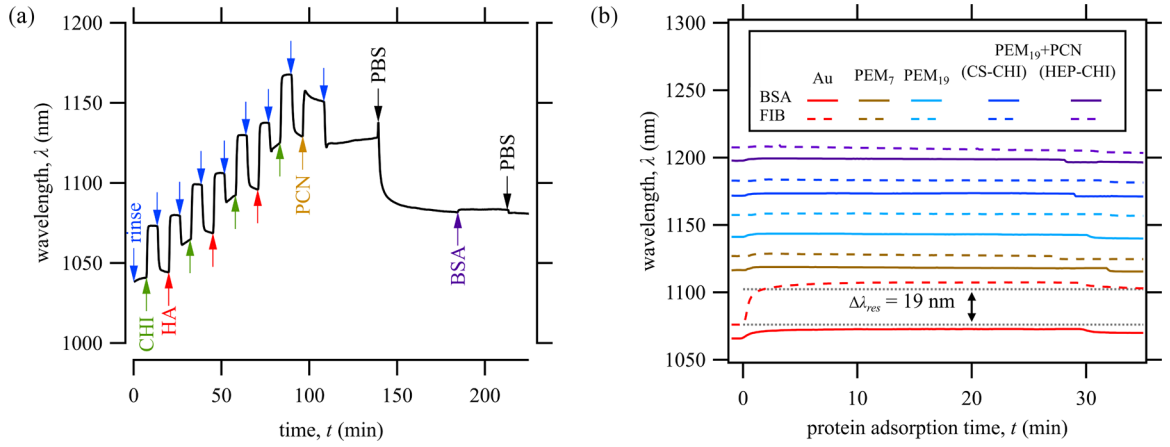


**Figure 3.** LbL assembly of PEM and protein adsorption from in situ FT-SPR. (a) Example of in situ FT-SPR data confirming the last seven layers of CHI-HA PEM assembly. These data show PCN adsorption, a subsequent rinse with PBS, and a 30 min BSA adsorption step. There is no measurable difference in wavelength before and after BSA adsorption. (b) BSA and FIB adsorption steps from in situ FT-SPR experiments. Irreversible protein adsorption is detected for both BSA and FIB on the control (gold-coated glass, modified with MUA self-assembled monolayer), but no irreversible adsorption of BSA or FIB adsorption is detected on any of the PEM or $PEM_{19}$ + PCN surface.

coatings. These coatings are within the evanescent field sensitivity of the SPR, evidenced by the change in the signal when the rinse solution is changed to PBS.

Models of protein adsorption on surfaces include both reversible and irreversible adsorption steps.[57−59] Irreversible adsorption is generally associated with protein aggregation or denaturation, which can lead to other longer-term and continuous changes in the surface chemistry, whereas reversible adsorption would likely lead ultimately to a dynamic equilibrium state, in which the surface is in equilibrium with the blood. On our PEM and $PEM_{19}$ + PCN, SPR does not detect irreversible adsorption, however, the SPR signal does change during the protein adsorption and subsequent rinse steps. SPR is extremely sensitive for detecting changes in both the thickness and the refractive index of the surface. Therefore, any change in the surface structure during protein adsorption, such as release of water and counterions, or desorption of polysaccharides may mask the detection of protein adsorption. Furthermore, the SPR technique requires that the surface be rinsed following adsorption, so that surface changes can be compared using the same refractive index background. To more precisely quantify protein adsorption phenomena without interference from other surface and solution changes, a technique that distinguishes reversible and irreversible protein adsorption while the surface is exposed to protein solution, is required.

**Protein Adsorption by Single-Molecule Fluorescence Microscopy.** To better quantify protein adsorption on bare glass (control), $PEM_7$, $PEM_{13}$, $PEM_{19}$, $PEM_{19}$ + PCN(CS-CHI), and $PEM_{19}$ + PCN(HEP-CHI), we conducted single-


DOI: 10.1021/acsami.8b09435
ACS Appl. Mater. Interfaces 2018, 10, 31892−31902

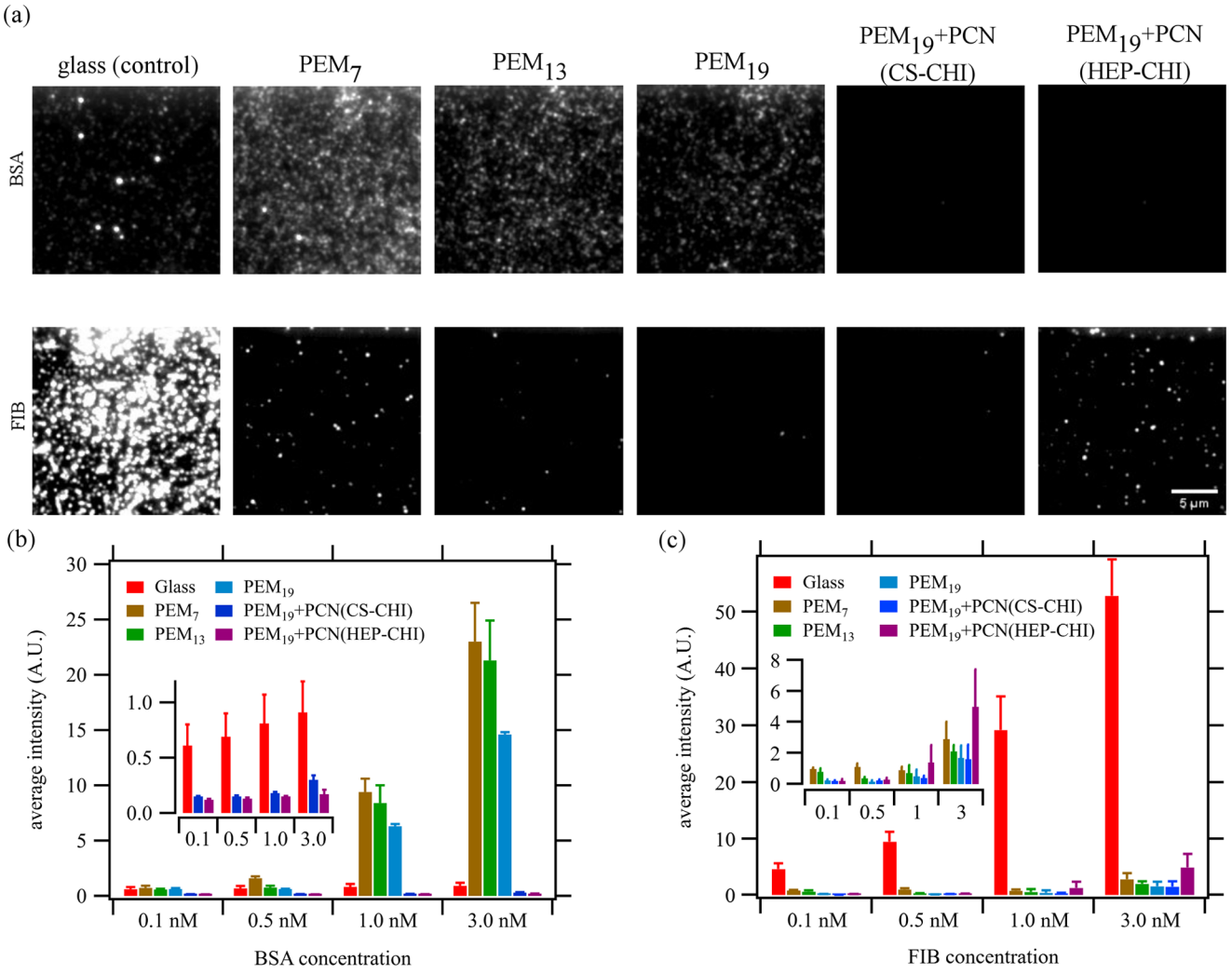


**Figure 4.** (a) Single-molecule fluorescence detection of BSA and FIB adsorption from 1 nM protein solutions on glass (control), 7-layer, 13-layer, 19-layer PEMs, and $PEM_{19}$ + PCN(CS-CHI) and $PEM_{19}$ + PCN(HEP-CHI) surfaces (scale bar is 5 $\mu$m). (b, c) Average fluorescence intensity from single-molecule fluorescence microscopy experiments at different protein concentrations. In (b) and (c) error bars represent standard deviation from experiments on three replicate surfaces ($n$ = 3). Insets in (b) and (c) show the data without the PEM samples (b) and without the glass control samples (c), so that the very low intensity signals can be compared.

molecule fluorescence microscopy using fluorescently labeled BSA and FIB (in these experiments, bare glass must be used as a control because the gold-coated glass control used for SPR cannot be used in TIRF microscopy). To enable single-molecule detection, proteins were diluted to very low concentrations (100 pM, 500 pM, 1 nM, and 3 nM) in pH 8.0 imaging buffer, as described in the Experimental Section. Imaging conditions (laser power, excitation angle, exposure time, etc.) were the same across all concentrations and surfaces. The lowest concentration of protein (100 pM) was allowed to equilibrate with each surface for 10 min. Then, microscopy videos were collected for 105 s (1000 frames) using oblique illumination to reduce background fluorescence. Subsequently, the protein solution concentration was incremented to the next concentration in the series (namely, 500 pM, 1 nM, and 3 nM), and the surface was again allowed to equilibrate for 10 min, before collecting 105 s of video. Separate surfaces were prepared for BSA and FIB. Figure 4a shows representative images obtained by averaging 1000 frames under oblique illumination during protein adsorption from the BSA and FIB solutions at 1 nM, after 10 min of incubation with the fluorescently labeled protein solution. Figure 4b,c also shows the mean fluorescence intensity of the adsorbed BSA and FIB on the surface of each experimental sample and the glass control, after 10 min of incubation with protein solution at different concentrations. When protein concentration is increased, the amount of adsorbed protein increases for all surface types. The clean glass control surface exhibits measurable adsorptions of BSA and FIB at all tested concentrations, as expected. When the glass is modified with chitosan-terminated PEM, the surface adsorbs more BSA than the glass, but the FIB adsorption is substantially reduced. For both proteins, the amount adsorbed decreases as the number of PEM layers increases for $PEM_7$, $PEM_{13}$, and $PEM_{19}$, as others have reported for polysaccharide-based PEMs.[35] Adding either the CS-CHI or HEP-CHI PCNs to make $PEM_{19}$ + PCN(CS-CHI) and $PEM_{19}$ + PCN(HEP-CHI) surfaces results in a substantial reduction in BSA adsorption (Figure 4), even though these surfaces have higher surface area (Figure 1). Interestingly, there is a significant difference between the CS-CHI and the HEP-CHI PCNs, with respect to FIB adsorption. At higher FIB concentrations (1 and 3 nM), the HEP-CHI


DOI: 10.1021/acsami.8b09435
ACS Appl. Mater. Interfaces 2018, 10, 31892−31902

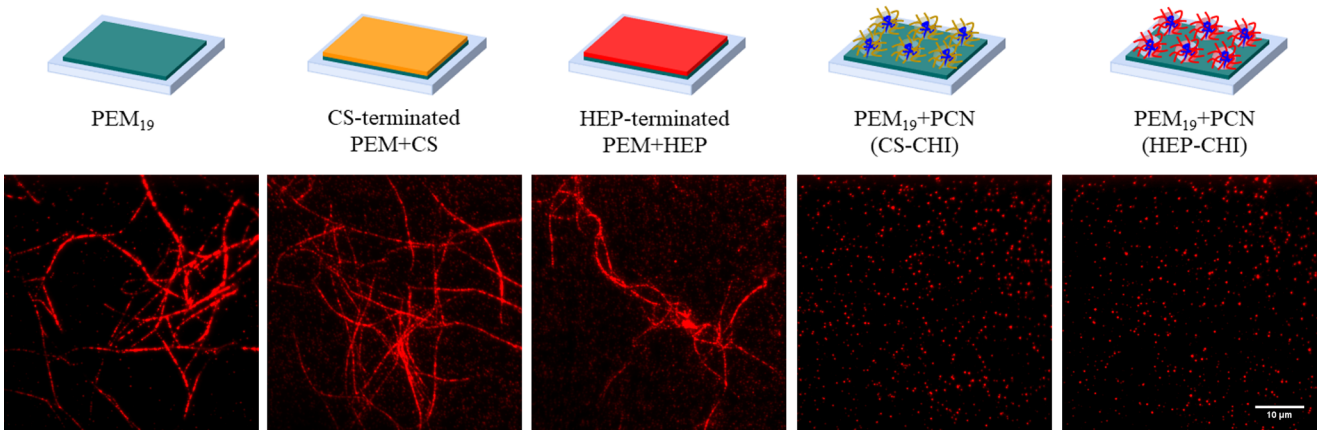


**Figure 5.** TIRF microscopy images of fluorescently labeled fibrin fibers, polymerized from physiologic concentration of fibrinogen (0.75 mg $mL^{-1}$), in the presence of thrombin (1 NIH U $mL^{-1}$) on PEMs. The structure of the $PEM_{19}$ + PCN samples does not prevent the adsorption of fibrin(ogen) monomers, but it completely prevents adsorption of fibrin fibers and fibrin polymerization on the surface.

PCN surface adsorbs more FIB than the CS-CHI PCN. This effect could be due to specific binding between heparin and FIB, as FIB is a heparin-binding protein.[60] The reduction in surface protein adsorption as the layer number increases, suggests that neither protein diffuses into the PEM. Rather, both proteins adsorb only on the surfaces. If the proteins were diffusing into the PEMs, then the amount of protein would increase as the PEM layer number increases.

**Fibrin Network Formation on Surfaces by Single-Molecule Fluorescence Microscopy.** Although the PCN-modified surfaces attract FIB, fibrin network formation is completely inhibited by the PCN structure. CHI-, CS-, and HEP-terminated PEMs and $PEM_{19}$ + PCN surfaces were exposed to a solution containing physiologic concentration of fibrinogen solutions (0.75 mg $mL^{-1}$), thrombin (at 1 NIH U $mL^{-1}$), and fluorescently labeled fibrinogen (5 nM). Thrombin converts FIB to the polymerizable fibrin, which then forms polymerized fibrin fibers. On the experimental surfaces, the first evidence of polymerized fibrin fibers appears after 30 min (see Figure S.3 in Supporting Information). After 40 min of incubation, total internal reflection fluorescence (TIRF) microscopy videos were collected on chitosan-terminated PEMs ($PEM_{19}$) (control), HEP-terminated PEMs (PEM + HEP), CS-terminated PEMs (PEM + CS), and PCN-terminated surfaces [$PEM_{19}$ + PCN(CS-CHI) and $PEM_{19}$ + PCN(HEP-CHI)]. TIRF videos were taken on a minimum of five different regions of three different surfaces, and one representative image is shown here for each surface type. In Figure 5, each image shows the average of 1500 frames after 40 min of incubation with the mixture of FIB and thrombin. These are the same fields of view shown in Figure S.3 in Supporting Information. A video of fibrin(ogen) interaction with PEM surfaces is also available in the Supporting Information.

On the $PEM_{19}$ surface (Figure 5), intersecting fibers suggest that a network of fibrin is formed on the control surface before 40 min, evidenced by visible intersecting fibers incorporating the fluorescently labeled fibrin(ogen). Similar fibrin networks are also observed on the PEM surfaces terminated with CS and HEP (PEM + CS and PEM + HEP). Therefore, coating the surface with heparin or chondroitin sulfate does not suppress fibrin polymerization on the surface or fibrin fiber adsorption from solution onto the surface. The formation of fibrin fibers and a crosslinked fibrin network is expected in these experiments because the only coagulation proteins present are fibrinogen and thrombin (e.g., there is no antithrombin III). Strikingly, in the cases of $PEM_{19}$ + PCN(CS-CHI) and $PEM_{19}$ + PCN(HEP-CHI), no fibrin fibers are observed on the surfaces, even after 40 min (Figure 5). For both types of $PEM_{19}$ + PCN surfaces, only sparse single molecules of fibrin(ogen) are adsorbed on the surface. Therefore, the $PEM_{19}$ + PCN surfaces must be inhibiting both fibrin fiber adsorption from solution and polymerization of fibrin on the surfaces. To further demonstrate the capacity of $PEM_{19}$ + PCN surfaces to inhibit fibrin network formation, a $PEM_{19}$ + PCN(CS-CHI) surface was incubated for 2 h with the same FIB/thrombin mixture. No fibers were observed on the surface even after 2 h (see Figure S.3 in the Supporting Information). This is remarkable since the $PEM_{19}$, PEM + CS, and $PEM_{19}$ + HEP surfaces all have obvious fiber formation after 30 min, and show intersecting fibers characteristic of fibrin networks, after only 40 min.

## DISCUSSION

Although some superhydrophobic surfaces, polymer brushes, and other surface chemistries can reduce protein adsorption to very low levels, no surface can completely eliminate all protein adsorption from a complex solution, containing many proteins, fats, sugars, cells, and polyvalent ions, such as blood.[34,36,55,56,61] When any biomaterial comes in contact with blood, a layer of nonspecifically adsorbed proteins will eventually form. Fibrin(ogen) and denatured albumin can bind platelets, promoting their attachment onto a biomaterial surface, ultimately leading to thrombus (blood clot) formation.[3,42,62,63] Fibrinogen on the surface of biomaterials can be converted to insoluble fibrin through thrombin-mediated cleavage of small fibrinopeptides A and B from the *N*-termini of the A$\alpha$ and B$\beta$ chains.[43−45] Activated fibrin molecules then polymerize into branched fibers, forming an elastic network, which traps red blood cells and ultimately forms a thrombus. On the inside surface of blood vessels, thrombin activity is inhibited by antithrombin III, which binds to sulfated glycosaminoglycans in the glycocalyx.[14] In this work, we show that in the absence of antithrombin III, sulfated GAGs ($PEM_{19}$ + PCNs) can inhibit fibrin network formation through a nanostructure-dependent mechanism, when they are presented in glycocalyx-mimetic bushlike domains formed by the PCNs.


DOI: 10.1021/acsami.8b09435
ACS Appl. Mater. Interfaces 2018, 10, 31892−31902

SPR is widely used to characterize protein adsorption when developing high-performance, ultralow fouling surfaces.[55,56] The PEM and glycocalyx-mimetic PEM + PCN surfaces proposed here are complex, multicomponent surfaces that can undergo multiple changes when exposed to different solution conditions, complicating interpretation of very small SPR signal changes. To overcome this limitation, we use single-molecule fluorescence microscopy to directly observe the interactions of blood proteins with PEM and glycocalyx-mimetic PEM + PCN surfaces. Like SPR, single-molecule fluorescence microscopy can be performed in real time. However, unlike SPR, the microscopy technique provides microscopic resolution of the protein interactions with the surface and distinguishes differences between PEM and $PEM_{19}$ + PCN surfaces. Furthermore, the SPR experiments also require a rinse step, so that the refractive index of the solution background is the same before and after protein adsorption. But in a long-term blood-contacting application, there is no periodic rinsing of the surface. Since the single-molecule fluorescence microscopy technique does not require that the surfaces be rinsed, these experiments provide detail about how proteins interact with the surface in a context that is more similar to a proposed blood-contacting application than the SPR experiments.

Models of protein adsorption on surfaces include both reversible and irreversible adsorption steps to describe these observed differences.[57−59] Single-molecule fluorescence microscopy also affords the ability to directly observe the formation of fibrin(ogen) fibers and fiber networks on the surfaces. The $PEM_{19}$ surface has very low fibrinogen adsorption (Figure 4). However single-molecule microscopy reveals that a fibrin fiber network still forms before 40 min on this surface when fibrinogen and thrombin are combined. The introduction of heparin or chondroitin sulfate on the surface (PEM + HEP and PEM + CS, Figure 4) is also not sufficient to prevent this fibrin network formation. However, $PEM_{19}$ + PCN have similarly low fibrinogen adsorption and also completely inhibit the fibrin network formation. The fibers and networks observed on the $PEM_{19}$, $PEM_{19}$ + HEP, and $PEM_{19}$ + CS are most likely a combination of fibers that polymerize from surface-adsorbed fibrin(ogen) and fibers formed in solution that subsequently adsorb. Neither of these phenomena occur on the $PEM_{19}$ + PCN surfaces. Polymerization of surface-bound fibrin(ogen) could be inhibited by PCNs on $PEM_{19}$ + PCN surfaces if the PCNs bind and isolate single fibrin(ogen) molecules, thereby suppressing their assembly to form fibers. In the TIRF videos (see Supporting Information) some sparse fibrin(ogen) molecules appear to be irreversibly bound while others appear and disappear from the TIRF plane of view, indicating adsorption and desorption. The adsorption of fibrin fibers from solution onto the $PEM_{19}$ + PCN surfaces may be inhibited by the surface topography introduced by the PCNs. The surface roughness of the $PEM_{19}$ + PCN, characterized by high $R_q$ and the 100−200 nm diameter hemispherical domains observed in the AFM images may restrict the relatively stiff fibrin fibers from conforming to the surface to form multiple adhesive contacts, thereby inhibiting adsorption.

The modification of surfaces with polysaccharide-based PEMs is a rapid, low-cost, and scalable process. Our group and others have demonstrated PEM modification of metals, polymers, composites (including bone tissue), and conformal coating of nanostructured materials.[4,47−49,53,54] Therefore, this simple strategy could be generalized to many blood-contacting medical devices to control the interactions of blood proteins with surfaces. We envision adapting these surfaces for materials for long-term blood-contacting applications, such as cardiovascular implants and extracorporeal blood circuits.

## CONCLUSIONS

Protein adsorption from blood is the initiating event in surface-induced blood clotting. Therefore, many researchers have proposed that ideal blood-contacting materials should be developed with a focus on reducing protein adsorption at the surface to prevent blood clotting.[3,5] The inside surface of blood vessels has overcome protein adsorption by developing a barrier on the endothelial cells, the endothelial glycocalyx, to maintain blood compatibility of the intravascular luminal wall. Rather than attempting to completely eliminate protein adsorption, we propose that mimicking the endothelial glycocalyx layer on the surface of biomaterials has the potential to suppress nonspecific blood protein adsorption. This approach represents a new paradigm in preventing blood clotting on biomedical device surfaces.

The glycocalyx-mimetic surfaces proposed here have no irreversible adsorption of BSA and FIB above the limit of detection of SPR. Single-molecule TIRF microscopy experiments show that the PCN in the $PEM_{19}$ + PCN surfaces inhibit both the surface-mediated polymerization of fibrin and the adsorption of fibrin fibers from solution, in the presence of thrombin. Further detailed investigation of how the structure and composition of these surfaces control protein−surface interactions in more complex protein solutions will enable elucidation of design principles for a new class of improved blood-contacting biomaterials based on mimics of the endothelial glycocalyx.

## ASSOCIATED CONTENT

### Supporting Information

The Supporting Information is available free of charge on the ACS Publications website at DOI: 10.1021/acsami.8b09435.

Theoretical background for PF-QNM, surface roughness ($R_q$), XPS and AFM analysis of surfaces, TIRF micrographs of fibrin(ogen) interactions with surfaces at the onset of fibrin fiber formation (30 min), and evidence of no fibrin(ogen) network formation on a $PEM_{19}$ + PCN(CS-CHI) surface following a two hour incubation of fibrinogen and thrombin (PDF)

Video from single-molecule TIRF microscopy of thrombin and fluorescently labeled fibrin(ogen) on glycocalyx-mimetic surfaces (MOV)

## AUTHOR INFORMATION

### Corresponding Author

*E-mail: mkipper@colostate.edu.

### ORCID

Melissa M. Reynolds: 0000-0002-1836-7324

Matt J. Kipper: 0000-0002-8818-745X

### Funding

This work was supported by the National Science Foundation (award numbers 1511830 and 1531921).

### Notes

The authors declare no competing financial interest.

## ■ ACKNOWLEDGMENTS

The authors thank Dr. Ellen Brennan-Pierce and Terrance Bishop for supporting the AFM instrument and Xinran Xu for his help with the microscopy measurements.

## ■ ABBREVIATIONS

AFM, atomic force microscopy; BSA, bovine serum albumin; CHI, chitosan; DLS, dynamic light scattering; FIB, fibrinogen; FT-SPR, Fourier transform surface plasmon resonance; GAG, glycosaminoglycan; HA, hyaluronan; HEP, heparin; MUA, 11-mercaptoundecanoic acid; PCN, polyelectrolyte complex nanoparticle; PDI, polydispersity index; PEM, polyelectrolyte multilayer; PF-QNM, peak force quantitative nanomechanics; TIRF, total internal reflection fluorescence; XPS, X-ray photoelectron spectroscopy

## ■ REFERENCES

(1) Jokinen, V.; Kankuri, E.; Hoshian, S.; Franssila, S.; Ras, R. H. A. Superhydrophobic Blood-Repellent Surfaces. *Adv. Mater.* **2018**, No. 1705104.
(2) Lavery, K. S.; Rhodes, C.; Mcgraw, A.; Eppihimer, M. J. Anti-Thrombotic Technologies for Medical Devices. *Adv. Drug Delivery Rev.* **2017**, *112*, 2−11.
(3) Liu, X.; Yuan, L.; Li, D.; Tang, Z.; Wang, Y.; Chen, G.; Chen, H.; Brash, J. L. Blood Compatible Materials: State of the Art. *J. Mater. Chem. B* **2014**, *2*, 5718−5738.
(4) Simon-Walker, R.; Romero, R.; Staver, J. M.; Zang, Y.; Reynolds, M. M.; Popat, K. C.; Kipper, M. J. Glycocalyx-Inspired Nitric Oxide-Releasing Surfaces Reduce Platelet Adhesion and Activation on Titanium. *ACS Biomater. Sci. Eng.* **2017**, *3*, 68−77.
(5) Reviakine, I.; Jung, F.; Braune, S.; Brash, J. L.; Latour, R.; Gorbet, M.; van Oeveren, W. Stirred, Shaken, or Stagnant: What Goes on at the Blood−Biomaterial Interface. *Blood Rev.* **2017**, *31*, 11−21.
(6) Reitsma, S.; Slaaf, D. W.; Vink, H.; van Zandvoort, M.; Egbrink, M. The Endothelial Glycocalyx: Composition, Functions, and Visualization. *Pflügers Arch.* **2007**, *454*, 345−359.
(7) Weinbaum, S.; Tarbell, J. M.; Damiano, E. R. The Structure and Function of the Endothelial Glycocalyx Layer. *Annu. Rev. Biomed. Eng.* **2007**, *9*, 121−167.
(8) Rostgaard, J.; Qvortrup, K. Electron Microscopic Demonstrations of Filamentous Molecular Sieve Plugs in Capillary Fenestrae. *Microvasc. Res.* **1997**, *53*, 1−13.
(9) Squire, J. M.; Chew, M.; Nneji, G.; Neal, C.; Barry, J.; Michel, C. Quasi-Periodic Substructure in the Microvessel Endothelial Glycocalyx: A Possible Explanation for Molecular Filtering? *J. Struct. Biol.* **2001**, *136*, 239−255.
(10) Hedayati, M.; Kipper, M. J. Atomic Force Microscopy of Adsorbed Proteoglycan Mimetic Nanoparticles: Toward New Glycocalyx-Mimetic Model Surfaces. *Carbohydr. Polym.* **2018**, *190*, 346−355.
(11) Leslie, D. C.; Waterhouse, A.; Berthet, J. B.; Valentin, T. M.; Watters, A. L.; Jain, A.; Kim, P.; Hatton, B. D.; Nedder, A.; Donovan, K.; et al. A Bioinspired Omniphobic Surface Coating on Medical Devices Prevents Thrombosis and Biofouling. *Nat. Biotechnol.* **2014**, *32*, 1134−1140.
(12) Olsson, P.; Lagergren, H.; Larsson, R.; Radegran, K. Prevention of Platelet-Adhesion and Aggregation by a Glutardialdehyde-Stabilized Heparin Surface. *Thromb. Haemost.* **1977**, *37*, 274−282.
(13) Lagergren, H.; Olsson, P.; Swedenborg, J. Inhibited Platelet Adhesion - Non-Thrombogenic Characteristic of a Heparin-Coated Surface. *Surgery* **1974**, *75*, 643−650.
(14) Larsson, R.; Olsson, P.; Lindahl, U. Inhibition of Thrombin on Surfaces Coated with Immobilized Heparin and Heparin-Like Polysaccharides - a Crucial Non-Thrombogenic Principle. *Thromb. Res.* **1980**, *19*, 43−54.
(15) Pasche, B.; Kodama, K.; Larm, O.; Olsson, P.; Swedenborg, J. Thrombin Inactivation on Surfaces with Covalently Bonded Heparin. *Thromb. Res.* **1986**, *44*, 739−748.
(16) Boddohi, S.; Kipper, M. J. Engineering Nanoassemblies of Polysaccharides. *Adv. Mater.* **2010**, *22*, 2998−3016.
(17) Wu, K. K.; Thiagarajan, P. Role of Endothelium in Thrombosis and Hemostasis. *Annu. Rev. Med.* **1996**, *47*, 315−331.
(18) Weber, N.; Wendel, H. P.; Ziemer, G. Hemocompatibility of Heparin-Coated Surfaces and the Role of Selective Plasma Protein Adsorption. *Biomaterials* **2002**, *23*, 429−439.
(19) Ito, Y.; Imanishi, Y.; Sisido, M. Invitro Platelet-Adhesion and Invivo Antithrombogenicity of Heparinized Polyetherurethaneureas. *Biomaterials* **1988**, *9*, 235−240.
(20) Park, K. D.; Kim, W. G.; Jacobs, H.; Okano, T.; Kim, S. W. Blood Compatibility of Spuu-Peo-Heparin Graft-Copolymers. *J. Biomed. Mater. Res.* **1992**, *26*, 739−756.
(21) Kim, Y. J.; Kang, I. K.; Huh, M. W.; Yoon, S. C. Surface Characterization and in Vitro Blood Compatibility of Poly(Ethylene Terephthalate) Immobilized with Insulin and/or Heparin Using Plasma Glow Discharge. *Biomaterials* **2000**, *21*, 121−130.
(22) Magnani, A.; Barbucci, R.; Montanaro, L.; Arciola, C. R.; Lamponi, S. In Vitro Study of Blood-Contacting Properties and Effect on Bacterial Adhesion of a Polymeric Surface with Immobilized Heparin and Sulphated Hyaluronic Acid. *J. Biomater. Sci., Polym. Ed.* **2000**, *11*, 801−815.
(23) Thorslund, S.; Sanchez, J.; Larsson, R.; Nikolajeff, F.; Bergquist, J. Bioactive Heparin Immobilized onto Microfluidic Channels in Poly(Dimethylsiloxane) Results in Hydrophilic Surface Properties. *Colloids Surf., B* **2005**, *46*, 240−247.
(24) Chen, J. L.; Li, Q. L.; Chen, J. Y.; Chen, C.; Huang, N. Improving Blood-Compatibility of Titanium by Coating Collagen-Heparin Multilayers. *Appl. Surf. Sci.* **2009**, *255*, 6894−6900.
(25) Tan, Q.; Ji, J.; Barbosa, M. A.; Fonseca, C.; Shen, J. Constructing Thromboresistant Surface on Biomedical Stainless Steel via Layer-by-Layer Deposition Anticoagulant. *Biomaterials* **2003**, *24*, 4699−4705.
(26) Lin, W. C.; Liu, T. Y.; Yang, M. C. Hemocompatibility of Polyacrylonitrile Dialysis Membrane Immobilized with Chitosan and Heparin Conjugate. *Biomaterials* **2004**, *25*, 1947−1957.
(27) Björck, C.-G.; Bergövist, D.; Esquivel, C. O.; Larsson, R.; Rudsvik, Y. In Vitro Evaluation of a Biologic Graft Surface. Effect of Treatment with Conventional and Low Molecular Weight (LMW) Heparin. *Thromb. Res.* **1984**, *35*, 653−663.
(28) Yang, M. C.; Lin, W. C. Protein Adsorption and Platelet Adhesion of Polysulfone Membrane Immobilized with Chitosan and Heparin Conjugate. *Polym. Adv. Technol.* **2003**, *14*, 103−113.
(29) Kito, H.; Matsuda, T. Biocompatible Coatings for Luminal and Outer Surfaces of Small-Caliber Artificial Grafts. *J. Biomed. Mater. Res.* **1996**, *30*, 321−330.
(30) Movafaghi, S.; Leszczak, V.; Wang, W.; Sorkin, J. A.; Dasi, L. P.; Popat, K. C.; Kota, A. K. Hemocompatibility of Superhemophobic Titania Surfaces. *Adv. Healthcare Mater.* **2017**, *6*, No. 1600717.
(31) Ippel, B. D.; Dankers, P. Y. W. Introduction of Nature's Complexity in Engineered Blood-Compatible Biomaterials. *Adv. Healthcare Mater.* **2018**, *7*, No. 1700505.
(32) de los Santos Pereira, A.; Sheikh, S.; Blaszykowski, C.; Pop-Georgievski, O.; Fedorov, K.; Thompson, M.; Rodriguez-Emmenegger, C. Antifouling Polymer Brushes Displaying Antithrombogenic Surface Properties. *Biomacromolecules* **2016**, *17*, 1179−1185.
(33) Buzzacchera, I.; Vorobii, M.; Kostina, N. Y.; de los Santos Pereira, A.; Riedel, T.; Bruns, M.; Ogieglo, W.; Möller, M.; Wilson, C. J.; Rodriguez-Emmenegger, C. Polymer Brush-Functionalized Chitosan Hydrogels as Antifouling Implant Coatings. *Biomacromolecules* **2017**, *18*, 1983−1992.
(34) Liu, Q.; Singh, A.; Lalani, R.; Liu, L. Ultralow Fouling Polyacrylamide on Gold Surfaces via Surface-Initiated Atom Transfer Radical Polymerization. *Biomacromolecules* **2012**, *13*, 1086−1092.


DOI: 10.1021/acsami.8b09435
*ACS Appl. Mater. Interfaces* 2018, 10, 31892−31902

(35) Wei, Y.; Hung, H.-C.; Sun, F.; Bai, T.; Zhang, P.; Nowinski, A. K.; Jiang, S. Achieving Low-Fouling Surfaces with Oppositely Charged Polysaccharides via LBL Assembly. *Acta Biomater.* **2016**, *40*, 16−22.
(36) Wörz, A.; Berchtold, B.; Moosmann, K.; Prucker, O.; Rühe, J. Protein-Resistant Polymer Surfaces. *J. Mater. Chem.* **2012**, *22*, 19547.
(37) Almodóvar, J.; Place, L. W.; Gogolski, J.; Erickson, K.; Kipper, M. J. Layer-by-Layer Assembly of Polysaccharide-Based Polyelectrolyte Multilayers: A Spectroscopic Study of Hydrophilicity, Composition, and Ion Pairing. *Biomacromolecules* **2011**, *12*, 2755−2765.
(38) Boddohi, S.; Killingsworth, C. E.; Kipper, M. J. Polyelectrolyte Multilayer Assembly as a Function of PH and Ionic Strength Using the Polysaccharides Chitosan and Heparin. *Biomacromolecules* **2008**, *9*, 2021−2028.
(39) Boddohi, S.; Moore, N.; Johnson, P. A.; Kipper, M. J. Polysaccharide-Based Polyelectrolyte Complex Nanoparticles from Chitosan, Heparin, and Hyaluronan. *Biomacromolecules* **2009**, *10*, 1402−1409.
(40) Place, L. W.; Sekyi, M.; Kipper, M. J. Aggrecan-Mimetic, Glycosaminoglycan-Containing Nanoparticles for Growth Factor Stabilization and Delivery. *Biomacromolecules* **2014**, *15*, 680−689.
(41) Boddohi, S.; Almodóvar, J.; Zhang, H.; Johnson, P. A.; Kipper, M. J. Layer-by-Layer Assembly of Polysaccharide-Based Nanostructured Surfaces Containing Polyelectrolyte Complex Nanoparticles. *Colloids Surf., B* **2010**, *77*, 60−68.
(42) Sivaraman, B.; Latour, R. A. The Adherence of Platelets to Adsorbed Albumin by Receptor-Mediated Recognition of Binding Sites Exposed by Adsorption-Induced Unfolding. *Biomaterials* **2010**, *31*, 1036−1044.
(43) Kattula, S.; Byrnes, J. R.; Wolberg, A. S. Fibrinogen and Fibrin in Hemostasis and Thrombosis. *Arterioscler., Thromb., Vasc. Biol.* **2017**, *37*, e13−e21.
(44) Riedel, T.; Suttnar, J.; Brynda, E.; Houska, M.; Medved, L.; Dyr, J. E. Fibrinopeptides A and B Release in the Process of Surface Fibrin Formation. *Blood* **2011**, *117*, 1700−1706.
(45) Weisel, J. W.; Litvinov, R. I. Mechanisms of Fibrin Polymerization and Clinical Implications. *Blood* **2013**, *121*, 1712−1719.
(46) Evans-Nguyen, K. M.; Schoenfisch, M. H. Fibrin Proliferation at Model Surfaces: Influence of Surface Properties. *Langmuir* **2005**, *21*, 1691−1694.
(47) Volpato, F. Z.; Almodóvar, J.; Erickson, K.; Popat, K. C.; Migliaresi, C.; Kipper, M. J. Preservation of FGF-2 Bioactivity Using Heparin-Based Nanoparticles, and Their Delivery from Electrospun Chitosan Fibers. *Acta Biomater.* **2012**, *8*, 1551−1559.
(48) Almodóvar, J.; Bacon, S.; Gogolski, J.; Kisiday, J. D.; Kipper, M. J. Polysaccharide-Based Polyelectrolyte Multilayer Surface Coatings Can Enhance Mesenchymal Stem Cell Response to Adsorbed Growth Factors. *Biomacromolecules* **2010**, *11*, 2629−2639.
(49) Lin, C.; Romero, R.; Sorokina, L. V.; Ballinger, K. R.; Place, L. W.; Kipper, M. J.; Khetani, S. R. A Polyelectrolyte Multilayer Platform for Investigating Growth Factor Delivery Modes in Human Liver Cultures. *J. Biomed. Mater. Res., Part A* **2018**, *106*, 971−984.
(50) Campagnola, G.; Nepal, K.; Schroder, B. W.; Peersen, O. B.; Krapf, D. Superdiffusive Motion of Membrane-Targeting C2 Domains. *Sci. Rep.* **2015**, *5*, No. 17721.
(51) Gervasi, M. G.; Xu, X.; Carbajal-Gonzalez, B.; Buffone, M. G.; Visconti, P.; Krapf, D. The Actin Cytoskeleton of the Mouse Sperm Flagellum Is Organized in a Helical Structure. *J. Cell Sci.* **2018**, No. jcs215897.
(52) Benesch, R. E.; Benesch, R. Enzymatic Removal of Oxygen for Polarography and Related Methods. *Science* **1953**, *118*, 447−448.
(53) Romero, R.; Chubb, L.; Travers, J. K.; Gonzales, T. R.; Ehrhart, N. P.; Kipper, M. J. Coating Cortical Bone Allografts with Periosteum-Mimetic Scaffolds Made of Chitosan, Trimethyl Chitosan, and Heparin. *Carbohydr. Polym.* **2015**, *122*, 144−151.
(54) Romero, R.; Travers, J. K.; Asbury, E.; Pennybaker, A.; Chubb, L.; Rose, R.; Ehrhart, N. P.; Kipper, M. J. Combined Delivery of FGF-2, TGF-B1, and Adipose-Derived Stem Cells from an Engineered Periosteum to a Critical-Sized Mouse Femur Defect. *J. Biomed. Mater. Res., Part A* **2017**, *105*, 900−911.
(55) Brault, N. D.; Sundaram, H. S.; Li, Y.; Huang, C.-J.; Yu, Q.; Jiang, S. Dry Film Refractive Index as an Important Parameter for Ultra-Low Fouling Surface Coatings. *Biomacromolecules* **2012**, *13*, 589−593.
(56) Hong, D.; Hung, H.-C.; Wu, K.; Lin, X.; Sun, F.; Zhang, P.; Liu, S.; Cook, K. E.; Jiang, S. Achieving Ultralow Fouling under Ambient Conditions via Surface-Initiated ARGET ATRP of Carboxybetaine. *ACS Appl. Mater. Interfaces* **2017**, *9*, 9255−9259.
(57) Rabe, M.; Verdes, D.; Seeger, S. Understanding Protein Adsorption Phenomena at Solid Surfaces. *Adv. Colloid Interface Sci.* **2011**, *162*, 87−106.
(58) Kim, J. Mathematical Modeling Approaches to Describe the Dynamics of Protein Adsorption at Solid Interfaces. *Colloids Surf., B* **2018**, *162*, 370−379.
(59) Krapf, D.; Campagnola, G.; Nepal, K.; Peersen, O. B. Strange Kinetics of Bulk-Mediated Diffusion on Lipid Bilayers. *Phys. Chem. Chem. Phys.* **2016**, *18*, 12633−12641.
(60) Mohri, H.; Ohkubo, T. Fibrinogen Binds to Heparin: The Relationship of the Binding of Other Adhesive Proteins to Heparin. *Arch. Biochem. Biophys.* **1993**, *303*, 27−31.
(61) Emilsson, G.; Schoch, R. L.; Feuz, L.; Höök, F.; Lim, R. Y. H.; Dahlin, A. B. Strongly Stretched Protein Resistant Poly(Ethylene Glycol) Brushes Prepared by Grafting-To. *ACS Appl. Mater. Interfaces* **2015**, *7*, 7505−7515.
(62) Sivaraman, B.; Latour, R. A. The Relationship between Platelet Adhesion on Surfaces and the Structure versus the Amount of Adsorbed Fibrinogen. *Biomaterials* **2010**, *31*, 832−839.
(63) Xu, L.-C.; Bauer, J. W.; Siedlecki, C. A. Proteins, Platelets, and Blood Coagulation at Biomaterial Interfaces. *Colloids Surf., B* **2014**, *124*, 49−68.


DOI: 10.1021/acsami.8b09435
*ACS Appl. Mater. Interfaces* 2018, 10, 31892−31902